Informatics in Medicine Unlocked 9 (2017) 191–199

Contents lists available at ScienceDirect

Informatics in Medicine Unlocked

journal homepage: www.elsevier.com/locate/imu

Assessment of calcified aortic valve leaflet deformations and blood flow dynamics using fluid-structure interaction modeling

Armin Amindari [a], Levent Saltik [b], Kadir Kirkkopru [a], Magdi Yacoub [c], Huseyin C. Yalcin [d,*]

[a] Faculty of Mechanical Engineering, Istanbul Technical University, Istanbul, Turkey
[b] Department of Pediatric Cardiology, Istanbul University, Cerrahpaşa Medical Faculty, Istanbul, Turkey
[c] National Heart & Lung Institute, Faculty of Medicine, Imperial College, London, UK
[d] Biomedical Research Center, Qatar University, Doha, Qatar

ARTICLE INFO

Keywords:
Aortic valve
Calcification
Computational fluid dynamics
Fluid-structure interaction
ANSYS
FLUENT
MECHANICAL APDL
Stenosis
Echocardiography

ABSTRACT

Aortic valve diseases are among the most common cardiovascular defects. Since a non-functioning valve results in disturbed blood flow conditions, the diagnosis of such defects is based on identification of stenosis via echocardiography. Calculation of disease parameters such as valve orifice area or transvalvular pressure gradient using echocardiography is associated with substantial errors. Computational fluid dynamics (CFD) modeling has emerged as an alternative approach for accurate assessment of aortic valve hemodynamics. Fluid-structure interaction (FSI) modeling is adapted in these models to account for counter-interacting forces of flowing blood and deforming leaflets for most accurate results. However, implementation of this approach is difficult using custom built codes and algorithms. In this paper, we present an FSI modeling methodology for aortic valve hemodynamics using a commercial modeling software, ANSYS. We simulated the problem using fluid flow solver FLUENT and structural solver MECHANICAL APDL under ANSYS and coupled the solutions using System Coupling Module to enable FSI. This approach minimized adaptation problems that would raise if separate solvers were used. As an example case, we investigated influence of leaflet calcification on hemodynamic stresses and flow patterns. Model geometries were generated using b-mode echocardiography images of an aortic valve. A Doppler velocity measurement was used as velocity inlet boundary condition in the models. Simulation results were validated by comparing leaflet movements in the simulations with b-mode echo recordings. Wall shear stress levels, pressure levels and flow patterns agree well with previous studies demonstrating the accuracy of our results. Our modeling methodology can be easily adopted by researchers that are familiar with ANSYS and other similar CFD software to investigate similar biomedical problems.

1. Introduction

Aortic valve separates the left ventricle from the aorta. It consists of three half-moon-shaped pocket-like flaps of leaflets housed within three sinuses [1]. A healthy aortic valve fully opens at ventricular systole and fully closes at ventricular diastole ensuring unidirectional flow with minimal regurgitation. The valve functions according to transvalvular pressure difference. Valve leaflets are exposed to complex hemodynamic forces during cardiac cycle: while the front ventricularis surfaces are exposed to unidirectional jet flows at peak systole, back fibrosa surfaces are exposed to circulatory flows while the valve is closing [2–4]. Valve calcification and bicuspid valve are the most common types of aortic valve defects. Incidence rate of congenital bicuspid valve is 0.5–2% [5]. Calcification affects mainly elderly with incidence rate of 2–7% in the population above 65 years of age [6].

Aortic valve defects prevent efficient opening of leaflets and result in aortic stenosis (AS), which is the formation of a high velocity jet at the valve orifice at peak systole. This disturbed flow condition also results in an increase in transvalvular pressure gradient (TPG) which is associated with heart attack risk [7]. Determination of jet velocity and TPG is essential for diagnosis of the condition. Doppler echocardiography is the most commonly used technique for that purpose. Doppler can measure the maximum blood velocity at the valve orifice, but not the axial velocity profile of the jet. The assumption of constant velocity along jet orifice will lead to some potential errors in further calculations for TPG [8]. Effective Orifice Area (EOA) is another parameter used by physicians for the clinical assessment of AS severity. EOA is the minimal cross sectional area of the aortic flow jet. EOA can be calculated from

* Corresponding author. Biomedical Research Center, Qatar University, PO Box 2713, Doha, Qatar.
E-mail address: hyalcin@qu.edu.qa (H.C. Yalcin).

https://doi.org/10.1016/j.imu.2017.09.001
Received 30 April 2017; Received in revised form 29 July 2017; Accepted 11 September 2017
Available online 15 September 2017

continuity equation by relating Doppler measured velocities at aortic valve inlet and at jet orifice [9]. Doppler velocities can be used to calculate TPG using simplified Bernoulli equation, where viscous terms are neglected. Due to simplifying assumptions and inaccuracy of the measurements, calculating EOA and TPG from Doppler velocities were shown to be associated with significant errors [10].

Accurate diagnosis of severity of aortic valve disease is crucial for therapy planning. However, as explained above, current approaches are associated with significant errors in hemodynamics analysis. Computational fluid dynamics (CFD) modeling has emerged as an alternative useful approach for elucidating complex cardiovascular flows where clinical measurement schemes would provide only limited information [11]. Patient-specific aortic valve CFD models are generated using medical images from patients [12]. These models enable a detailed disturbed flow analysis and precise determination of defect severity. Disturbed hemodynamics can trigger mechano-biological mechanisms (i.e. up/down regulation of gene expressions etc.) leading to further complications [13]. Therefore, qualitative and quantitative hemodynamics analysis for defected aortic valves will be important in biological investigation of the disease as well.

There are numerous previous numerical studies on aortic valve hemodynamics [14–16]. The initial studies focused on the investigation of blood flow and determination of hemodynamic force levels on the leaflets at a specific time point in the cardiac cycle (in most cases ventricular systole) using static geometries. In these studies, only the structural domain (aortic root and leaflets) was modeled and fluid flow behavior through the valve was excluded. Grande et al. generated 3D finite element models from MRI images using ANSYS and defined physiological pressure on the leaflets as boundary condition [17]. The study showed that, patient specific asymmetries are important in stress distribution on the aortic root and the leaflets. With the current advancements in simulation techniques and computational speeds, dynamic leaflet movements could be modeled in more recent studies. Weinberg et al. developed 3D aortic valve models using LS-Dyna and defined transient dynamic hydrostatic pressure on the structural zones as the boundary condition in the models [18]. Influence of valve calcification on leaflet movement behavior was investigated in the study. In a more recent investigation on calcification, patient specific 3D models were generated from MRI images of aortic valve patients. Using ABAQUS software, transient pressure boundary condition was applied on the leaflets [19]. The valve orifice area decreased when calcification level increased in the study.

These studies contributed substantially to our understanding of the aortic valve behavior during disease. However, such structural models cannot be used to investigate disturbed hemodynamics, which was shown to be important in the progression of aortic valve disease. Aortic valve behavior is a complex dynamic event since it involves both fluid and structure movements. To model this complex dynamic problem, fluid-structure interaction (FSI) approach should be adapted. In this approach, valve leaflets are modeled as deformable structural domain and blood flow is modeled as fluid domain. Two domains are coupled and mathematical solutions of the fields are determined simultaneously. This approach enables researchers to investigate the dynamics of leaflet movements and blood flow throughout the cardiac cycle in a reliable manner.

In a pioneering FSI study by De Hart et al., aortic valve hemodynamics was modeled in 2D and associated fluid and structure equations were solved simultaneously using custom algorithms developed by the authors [20]. In another study, ADINA commercial software was utilized for generating 2D FSI models to investigate hemodynamic forces on bicuspid and tricuspid aortic valves [21]. Here, transient pressures on the leaflets were used as boundary condition and the solution was converged when the solution approximated physiological values. In more recent studies, aortic valve hemodynamics was simulated in 3D. Halevi et al. investigated the influence of calcification on valve hemodynamics using 3D FSI models [22]. Here, structural model was generated using ABAQUS and flow field was solved using Flow Vision. Fedele et al. developed a patient-specific FSI modeling approach based on moving resistive immersed implicit surfaces [14]. Here, a mathematical model was generated to represent a fluid in a general domain with an immersed structural domain into the fluid domain. FSI approach was adapted to evaluate the performances of aortic valve replacements as well. Yun et al. investigated the blood damage through bi-leaflet mechanical aortic valves [23] and Vahidkhah et al. studied blood stasis on prosthetic aortic valves using such 3D FSI models [24]. These studies were very important FSI modeling examples of the aortic valve. Advanced mathematical modeling approaches adapted in most of these studies make them difficult to be adopted by other researchers.

In this study, we aimed to simulate aortic valve hemodynamics in a practical and reliable way, that would make the models easily adoptable by others. For this purpose, we generated 2D FSI aortic valve models under a single modeling platform, ANSYS. Fluid and structure fields were defined on patient specific models that were prepared in ANSYS Workbench. ANSYS FLUENT and ANSYS MECHANICAL APDL were used to solve fluid and structure fields respectively. Two fields were coupled using System Coupling FSI Module in ANSYS Workbench. Since all the solvers and modules work under one platform, adaptation problems that might raise due to utilization of separate software packages and modules were minimized. The influence of leaflet calcification on flow and leaflet movement dynamics was investigated using this approach. The modeling technique that we developed in this study will be readily adoptable to researchers using ANSYS for heart valve modeling.

2. Methods

In this study, we simulated aortic valve hemodynamics using ANSYS package program. For this purpose, we generated a 2D model geometry based on aortic valve images from a patient. Surfaces and regions in the geometry were defined appropriately to allow FSI. Simultaneous solutions were obtained for fluid and structure zones using separate solvers under ANSYS WORKBENCH. Below, we summarize our solution steps in detail:

2.1. Echocardiography imaging

Aortic valve from a healthy individual at 27 years old was imaged via echocardiography using 7 and 3 MHz scanners (GE Vivid 7 Ultrasound Machine). Dimensions of the valve (i.e. inlet, orifice, sinus and root diameters) were measured from short axis b-mode images (Fig. 1A). Time dependent velocity profile at the aortic valve inlet was measured via Pulsed Doppler Mode (Fig. 1B, left). These velocity measurements were used as transient velocity boundary condition for the simulation (Fig. 1B, right).

2.2. Numerical model

The geometry of the model was developed in ANSYS Workbench based on b-mode measurement data (Fig. 1C). The numerical model is divided to two separate fields: The flow field and the Structure Field.

The flow field consists of blood inlet surface, blood outlet surface and the blood flow region. Inlet surface of the geometry (left surface in Fig. 1C) was defined as velocity inlet boundary condition. The velocity profile for aortic valve inlet was measured using Doppler technique and applied as the transient velocity boundary condition on this surface. Flow at the inlet was assumed plug flow [25]. At a specific time-point, inlet velocity is the spatially averaged velocity of the blood flow entering to the aortic valve from left ventricle. This average value equals to the maximum axial velocity measured by Doppler at valve inlet (plug flow assumption). The transient velocity profile was defined as an UDF file to be interpreted by FLUENT solver. This file includes the transient velocity data for inlet surface for each time step. The outlet surface (right surface in Fig. 1C) was defined as pressure outlet and the outlet pressure was set

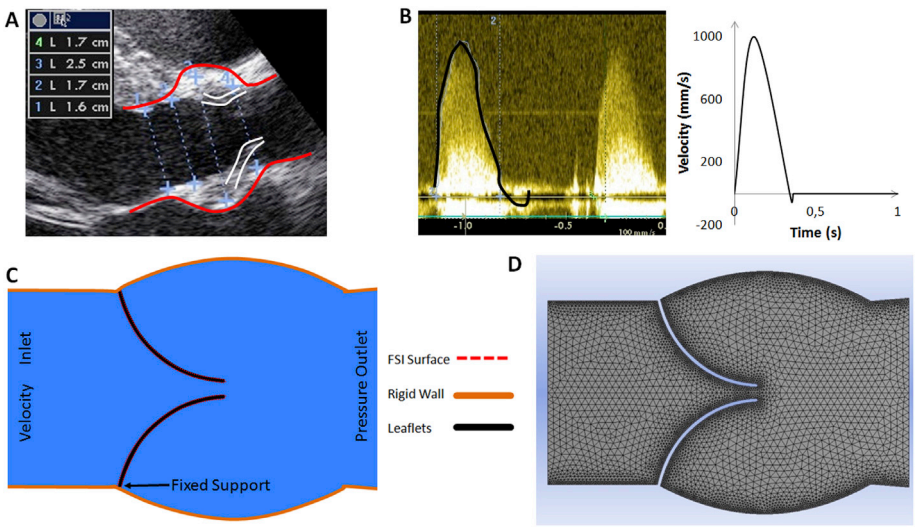

Fig. 1. Model geometry generation. A. Dimensions of an aortic valve were determined from the short axis b-mode views. B. Doppler velocity measurements for the same valve (left) were defined as the inlet transient velocity boundary condition (right) in the model. C. Geometry was generated in ANSYS Workbench and boundaries and zones are defined. D. Fluid zone (blood flow) and structure zone (leaflets) are meshed separately.

to gauge pressure value of zero. It has been assumed that there is no heat transfer between the blood flow and the arteries. The blood flow field was discretized into prism elements using sweep method. An unstructured mesh was generated for the fluid with a denser mesh near wall and leaflet surfaces to capture high velocity gradients in the boundary layers (Fig. 1D) with a maximum skewness of 0.84. A mesh convergence study was performed at steady state peak velocity to determine optimum mesh density. We observed that the accuracy of the solution does not change for models with more than 10,000 prism elements.

The structure field consists of rigid walls, and flexible valve leaflets. Rigid wall surfaces consist of artery walls and aortic root (upper and lower boundaries in the geometry). Aortic root wall surfaces were defined as rigid wall for simplicity and no slip boundary condition was applied on these surfaces. Joints between leaflets and walls were defined as fixed supports. A uniform mesh was generated for the leaflets using tetrahedral elements. A mesh convergence study was performed at steady state by applying constant pressure on leaflets. We observed that the accuracy of the solution does not change for models with more than 100 structure elements. The skewness of the elements was kept below 0.6 to ensure convergence and accuracy of the solution.

Blood flow forces causes large deformations of the leaflets. Hence the surface between blood and leaflets were defined as FSI surfaces. No slip boundary condition was also applied for these FSI surfaces.

2.3. Solution of the fluid equations

In this study, the governing equations of the fluid field were solved using commercial package program FLUENT. The blood flow was assumed to be incompressible with constant blood density of 1060 kg/m^3. Due to incompressible nature of the flow, the pressure-based solver was adapted. Here, the velocity field is obtained from momentum equations, and the pressure field is extracted from a pressure correction equation, which is obtained by relating continuity and momentum equations. The blood was assumed Newtonian with constant viscosity of 0.0035,578 J/s. The details of the continuity and the momentum equations can be found in Ref. [26]. Second order Upwind Scheme was used for spatial discretization of momentum and turbulence equations within fluid zone [27].

Peak Reynolds number in the simulations is around 2804. Besides, the modeled flow is pulsatile in character and we have a complex and dynamic geometry. Therefore, we expect to have turbulence flow downstream of the aortic valve. For turbulence modeling, k-ε realizable turbulence model was utilized, which is a two-equation RANS model. Compared to standard k-ε model, realizable k-ε model predicts the spreading rate of the both planar and round jets more accurately and gives more realistic results for flows involving flow separation and circulatory flow regimes [28]. Realizable k-ε model introduces an improved transport equation for turbulent dissipation rate.

Prior to defining boundary conditions for k-ε realizable model, turbulence intensity value must be set for the problem. Turbulence intensity depends on the Reynolds number and a default value of 1.5% was defined for our simulation based on previous studies in the literature [29]. Standard wall functions were used near wall regions in order to accurately model physical behavior in these viscous boundary layers. Second order Upwind Scheme was used for spatial discretization of momentum and turbulence equations within fluid zone [26].

2.4. Solution of the deformation equations for leaflet movements

The dynamic response of leaflets for time-dependent blood flow forces is modeled using ANSYS MECHANICAL APDL, Transient Structural solver. The module enables calculating transient forces, displacements, strains, and stresses, on the leaflets. ANSYS program uses Newmark time integration method to solve these equations at discrete time-points. Here, the time increment between successive time-points is called the integration time step. Before running the simulation, grid information of the structural leaflet zones is imported to the solver and mechanical properties of these zones are defined. These properties are Young modulus of elasticity, Poisson ratio and density. The density of the leaflets was set at 1060 kg/m^3 and is equal to blood density [30]. Leaflets were modeled as isotropic linear elastic material. Young moduli of the leaflets were assigned to define healthy and calcified cases: 2 MPa for a healthy valve, 10 MPa for a moderately calcified case, and 20 MPa for a severely calcified case [31]. The Poisson's Ratio of the leaflets are set at 0.3 [32].

2.5. FSI coupling

For deformations with strong physical interactions, 1-way uncoupled approach is not recommended and 2-way coupled approaches are more suitable [33]. 2-way couplings can be further classified as implicit and explicit approaches. For problems with strong physical interactions, explicit methods give poor results [34]. Therefore, for analysis involving highly deformable biological structures, 2-way couplings with implicit approach needs to be adapted due to presence of strong interactions. The

ANSYS Coupling Module uses iterative implicit 2-way coupling approach to solve the numerical FSI problems. This method overcomes limitations including intensive computational memory and long solution time requirements. In this approach, solution time is discretized into finite time-steps. For the first time step, domains are spatially discretized, and governing equations are solved for each discrete time. Once the interactions between the fields are converged, the solution fields are obtained for this time-point. These solutions are the initial values for the following time-step. Following the new discretization of the domains for the new time step, equations are solved again. This way, separate solution fields are calculated for all of the time-steps [35].

In this work, ANSYS® Academic Research, Release 16.2 was utilized to perform iterative implicit coupled analysis for modeling the interactions between the blood flow and the leaflet movements of the aortic valve. Here, flow field and structure field are solved separately. For ANSYS, Workbench is the platform within which different numerical solvers can be connected. Adapting this method, the blood flow field was solved with FLUENT solver. Leaflet deformations on the other hand was solved with Mechanical APDL, transient structure solver within ANSYS. In each time step, Continuity, Navier-Stokes and Turbulence equations governing the blood flow were solved in FLUENT and leaflet deformation equations were solved in M-PADL solver. Two data transfers are needed during the analysis. First data transfer is the force data from FLUENT solver to M-APDL solver for the specific step. Details of this method can be found in the study by Galpin et al. [36]. Using this data for this time step, the equations governing the deformation of the leaflets are solved. Second transfer is the displacement quantity data transfer from M-APDL solver to FLUENT solver. The details of this method are presented in the study by Jansen et al. [27]. With the deformed leaflet configuration, fluid equations are solved for the later time step and coupled solutions continue. This way, solution is marched in time. Coupling approach is summarized in Fig. 2A. Co-simulation workflow was used to run both solvers simultaneously while exchanging data. This workflow for co-simulation of 2-way FSI analysis is set up in Workbench (Fig. 2B). The geometry is shared between FLUENT and M-APDL solvers. Using a single geometry for the solvers will ensure that FSI surfaces match smoothly.

Total solution time was divided into time-steps, each having 6e-5 s duration. Each time-step consists of 5 coupling iterations. These values (i.e. duration of a time-step and number of iterations for each time-step) were determined based on enhanced solution stability. To prevent incompatibility between fluid and structure fields, FSI surfaces for blood and leaflets must be paired. For this purpose, nodes of the blood field for receiving leaflet displacements information and nodes of leaflets field for receiving blood force data must be mapped at the start of processing.

2.6. *Remeshing of the fluid zone*

In the simulations, blood flow exerts dynamic forces on leaflets, which causes large deformations of these structures. Leaflets movements are within flow domain and these movements deteriorate flow zone. Therefore, for each time step, flow domain needs to be re-discretized to enhance mesh quality. Spring-based smoothing and remeshing algorithm in FLUENT was utilized to minimize grid problems due to high leaflet deformations. The details of this method can be found in the user manual by ANSYS [35]. This method is suitable for meshes, which do not distort significantly. On the other hand, when the boundary displacement is large compared to the local cell sizes, cell quality can deteriorate. In other words, cells may become degenerative. This will invalidate the mesh (negative cell volumes) and, will lead to convergence problems when the solution is updated to the next time step. To circumvent this problem, cells that violate the skewness or size criteria are identified and these are locally remeshed. Once the cells or faces satisfy the skewness criteria, the mesh is locally updated with the new cells.

3. Results

3.1. *Model validation*

Computational model was validated by comparing leaflet deformation in the simulation with b-mode echo images for the aortic valve that

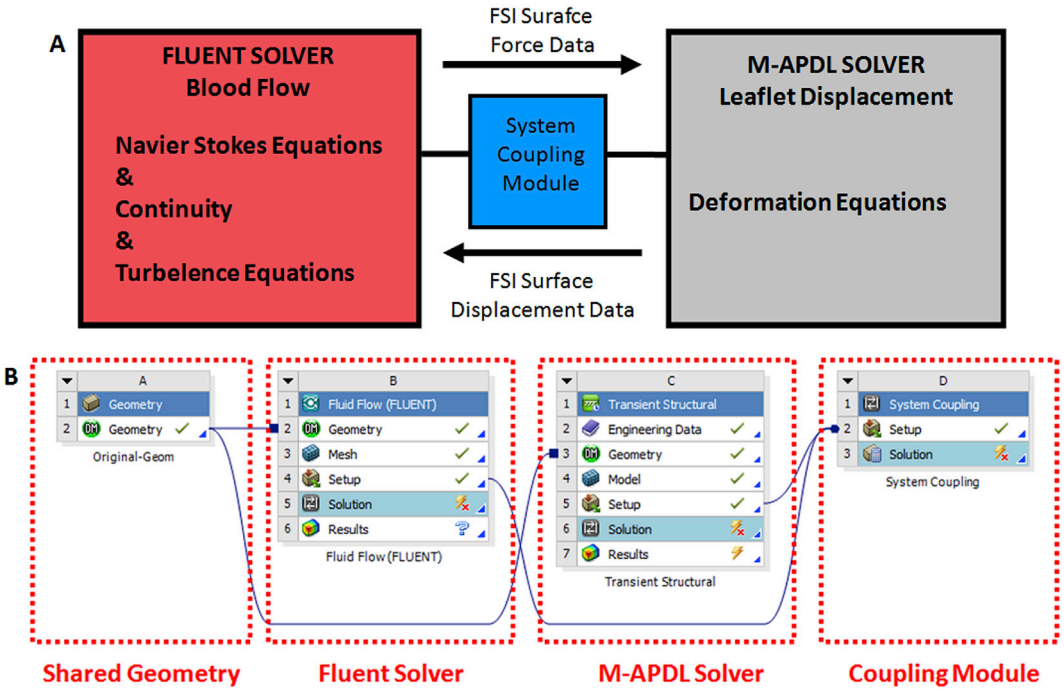

Fig. 2. Adapted FSI approach using System Coupling Module in ANSYS Workbench. A. 2-way implicit solution approach in ANSYS. Total analysis time is divided into finite time-steps. In each time-step, Continuity, Navier-Stokes and Turbulence equations governing the blood flow were solved in FLUENT and leaflet deformation equations were solved in M-PADL solver. First data transfer is the force data from FLUENT solver to M-APDL solver for the specific step. Second transfer is the displacement quantity data transfer from M-APDL solver to FLUENT solver. B. The workflow for co-simulation 2-way FSI analysis in ANSYS Workbench. This workflow consists of Geometry Component System, Fluid Flow Analysis System (FLUENT), Transient Structural Analysis System (M-APDL) and System Coupling Component System. The geometry is shared between FLUENT and M-APDL solvers.

was used to generate the model (healthy case). Fig. 3 shows leaflet orientations in the b-mode echo images and in the simulation for ventricular diastole, systole and closure stages. Simulation results agree well with echo images showing the adapted FSI modeling approach works accurately. To further validate our models, we calculated time averaged WSS on the leaflets and maximum TPG values in the healthy valve simulation and compared these with previous studies. Average WSS was 8.7 Pa and maximum TPG was 633 Pa. These values are in agreement with previous findings (7.9 Pa WSS and 799 Pa TPG) [37–39].

3.2. Velocity contours, velocity streamlines and velocity vectors throughout cardiac cycle for the health valve model

Fig. 4 shows the velocity contours for the healthy valve model throughout cardiac cycle. At peak systole (0.08 s–0.1s), axial velocity gradients near the ventricularis surface of the valves are very high indicating high WSS on these surfaces. After a high jump near the ventricularis surface, axial velocity does not change much within the jet orifice indicating plug flow profile for the jet. Maximum velocity is localized to the valve orifice as expected. Fig. 5 shows the velocity streamlines for the healthy valve model throughout cardiac cycle. Streamline patterns clearly identifies high velocity jet flow at the valve orifice at systole and circulatory flows in the sinuses at late cycle (shown with arrows). Fig. 6 represents the velocity vectors throughout cardiac cycle, focusing on late cycle. Velocity vectors clearly identifies circulatory flows as the leaflets starts to close (>0.1s). Vortices are in one direction and do not reverse as the leaflets move, indicating WSS in aortic surface of the leaflets are unidirectional and are not oscillatory. This result is in agreement with a similar recent study [2].

3.3. Effects of leaflet calcification on leaflet movements, flow dynamics and stress levels

As explained in the methods section, leaflet Young Modulus for the healthy, calcified and severely calcified cases are, 2 MPa, 10 MPa and 20 MPa respectively based on previous studies [40]. Fig. 7 displays velocity contour, velocity streamline and velocity vector snapshots at peak systole for the models. From the top snapshots of velocity contours, calcification prevents efficient opening of the leaflets and results in stenosis. We defined a parameter, opening ratio, to quantify amount of stenosis. This parameter is the percentage of orifice diameter to root diameter. Orifice diameters were found to be 14 mm for healthy model, 10.5 mm for calcified model and 9 mm for severely calcified model. Corresponding opening ratios were 70%, 52.5% and 45%. Calcification resulted in an increase in peak orifice velocity from 1.57 m/s for health case to 2.18 m/s for calcified case and to 2.38 m/s for the severely calcified case.

Fig. 7 middle snapshots displays velocity streamlines at peak systole for the three models. Jet type parallel streamline flows in the valve orifice are present for the models. In the sinuses, vortices are present for all the cases. Shape, location, and strength of the vortices were all affected by calcification severity level. Near the annulus of the valve, along the base of the sinus and leaflet, there is significantly more flow for the healthy valve compared to calcified valves. The vortices are bigger in size in calcified cases. These results are in agreement with similar studies [41]. (See streamline animations for complete cardiac cycles for three models as supplemental movies). Fig. 7 bottom snapshots represent velocity vectors at peak systole for the models. The existence of clockwise vortices in bottom sinus and counterclockwise vortices in upper sinus of all three cases can be verified from velocity vectors.

Supplementary video related to this article can be found at https://doi.org/10.1016/j.imu.2017.09.001.

We next calculated pressure values to evaluate TPG for the models. Fig. 8, top three snapshots are the absolute pressure contours at peak systole. Calcification results in a significant increase in TPG, from 633 Pa (~5 mmHg) for the healthy case, to 1995 (~15 mmHg, %188 increase) for the calcified case and to 2559 (~19 mmHg, %305 increase) for the severely calcified case. These values are in agreement with case studies of patients with valvular heart disease [42].

WSS levels on the leaflets at peak systole for the three models are compared in Fig. 8 bottom snapshots with octahedron representation. WSS is the frictional force on the leaflets and is simply the product of dynamic viscosity of the fluid (μ) and normal velocity gradient at the wall. As seen from the figure, calcification increases WSS on the leaflets significantly and tips of the leaflets are exposed to highest WSS for all cases. Area weighted average WSS at peak systole (front ventricularis and back aortic surface values are averaged together) is 13.3 Pa for the healthy valve model, 17.5 Pa for the calcified model (% 32 increase) and 22.5 PA for the severely calcified model (%69 increase). For all the models, WSS levels increase toward tip of the leaflets. These results are consistent with previous findings [2,43]. We also calculated time averaged and maximum WSS levels for the models. Our findings for WSS

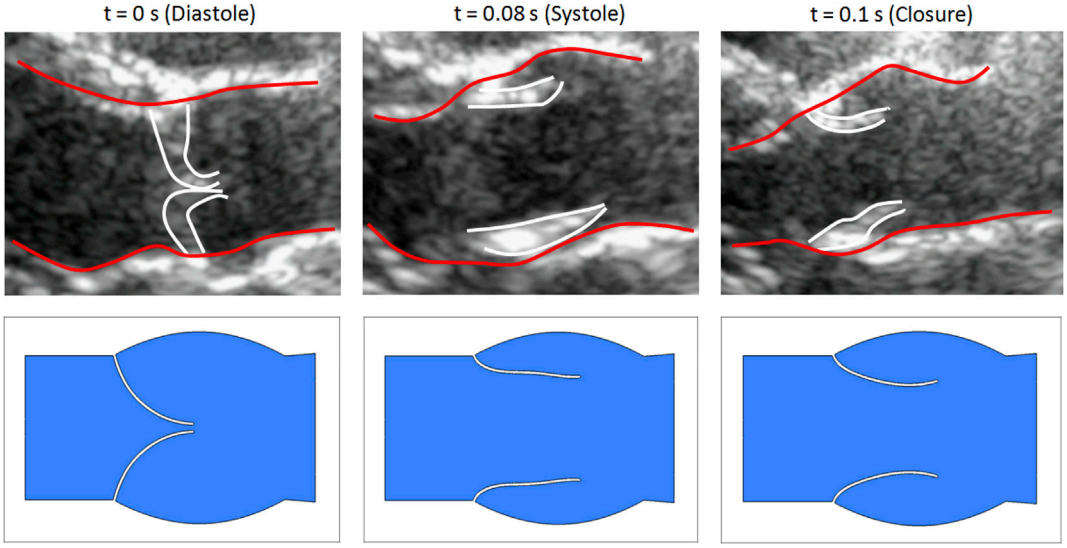

Fig. 3. Comparison of simulation leaflet deformations with b-mode echo images. Upper images are long axis b-mode echo images for the healthy aortic valve at ventricular diastole, systole and closure stages. Lower images are snapshots from the healthy valve simulation for the same stages with echo images. Edges of the leaflets are traced with white and aortic root is traced with red in echo images. Leaflets movements in the simulation are consistent with movements from echo images at respective stages.

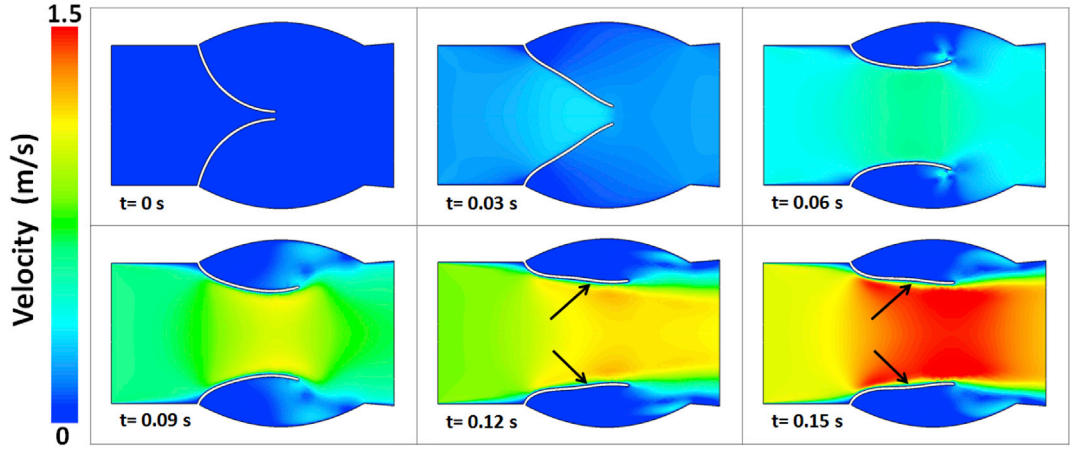

Fig. 4. Velocity contours for the healthy valve model at different time-points in the cardiac cycle. High velocity jet acting on the front ventricularis surface of the leaflets can be seen clearly (shown with arrows).

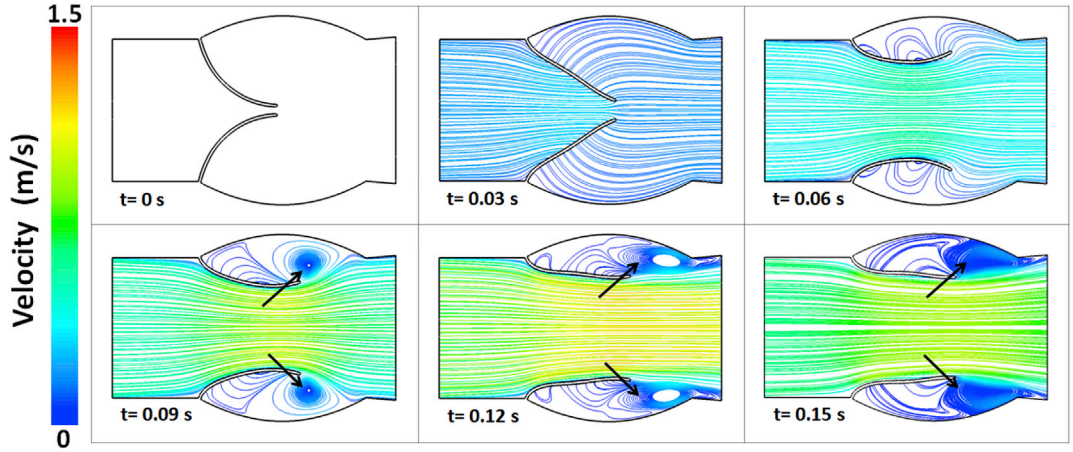

Fig. 5. Velocity streamlines for the healthy valve model at different time-points in the cardiac cycle. High velocity jet flow at the valve orifice at systole and circulatory flows in the sinuses at late cycle (shown with arrows) can be seen clearly.

along with other calculated parameters for the models are summarized in Table 1.

Previous studies suggested that, the differences in WSS levels in front and back sides of the leaflets also influence formation of calcification [44,45]. To reveal stress variations in our models, we calculated WSS levels on ventricularis and fibrosa sides separately. For the healthy model, spatially-averaged WSS at peak velocity on front ventricularis surface is 27.5 Pa and on back fibrosa surface is 18.3. For the calcified model, these values are 39.7 Pa and 5.1 Pa and for the severely calcified model these are 46.5 Pa and 4.5 Pa. According to these results, as the

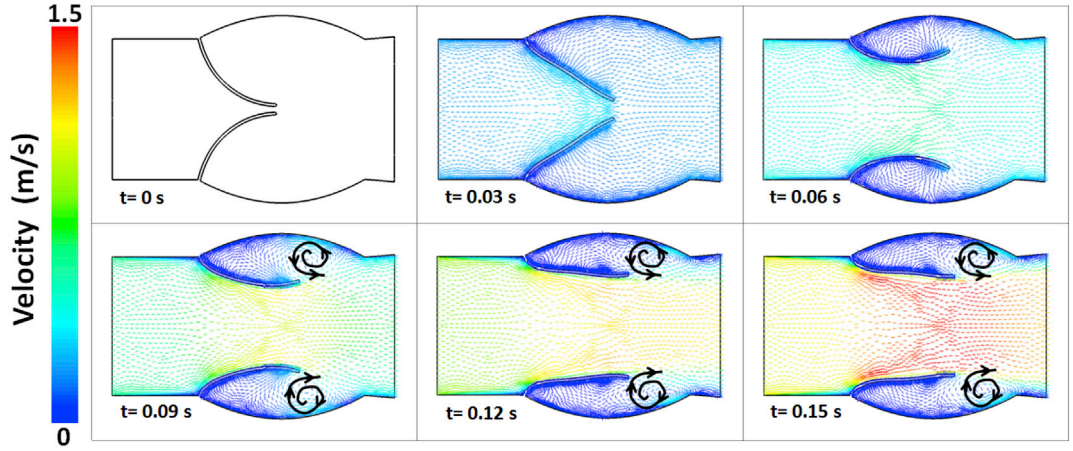

Fig. 6. Velocity vectors for the healthy valve model at different time-points in the cardiac cycle. Velocity vectors clearly identifies circulatory flows as the leaflets starts to close (>0.1s). Vortices are in one direction (shown with arrows in upper sinuses) and do not reverse as the leaflets move, indicating WSS in aortic surface of the leaflets are unidirectional.

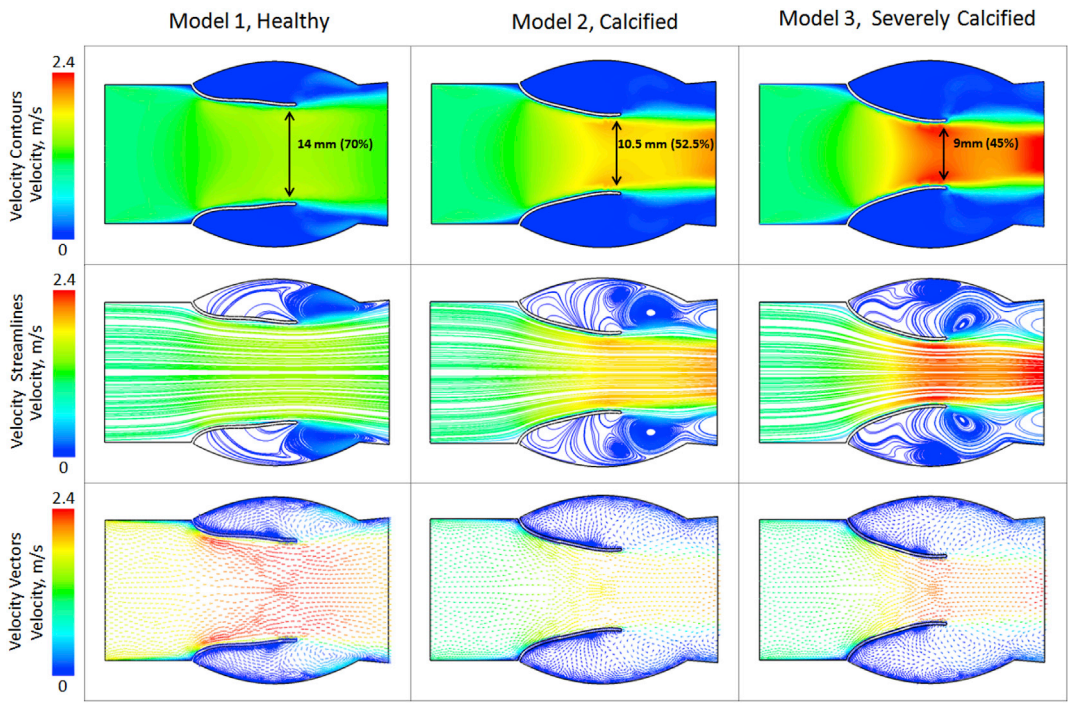

Fig. 7. Velocity contours, velocity streamlines and velocity vectors at peak systole for healthy, calcified and severely calcified models. Top three snapshots are velocity contours for the models. Calcification results in stenosis and increase in orifice jet velocity as expected. Opening ratio decreased from 70% for the health valve model to 45% in the severely calcified case. Middle three snapshots are velocity streamlines for the models. Calcification results in growth of circulatory flow regions in the sinuses. Bottom three snapshots are velocity vectors for the models. Circulatory flows in the sinuses can be seen clearly in all the models.

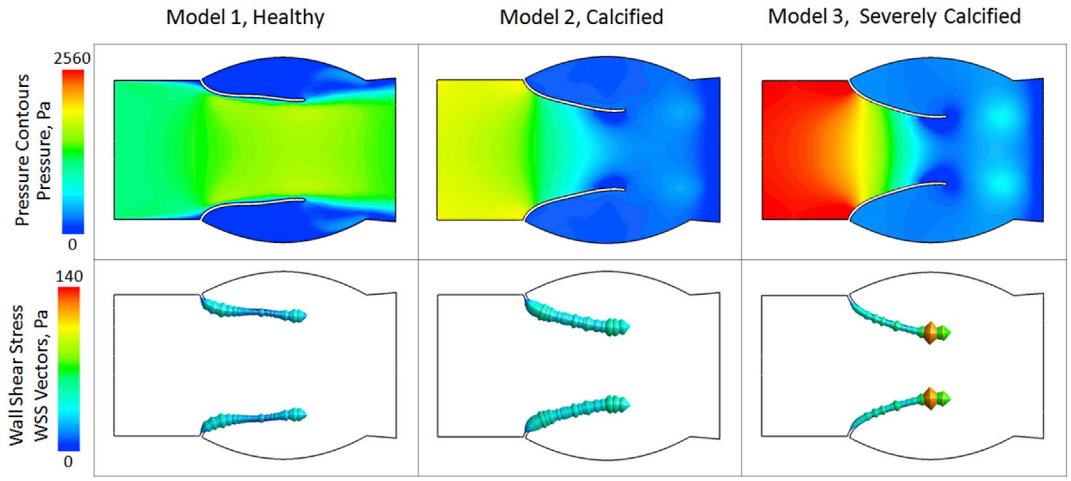

Fig. 8. Pressure and WSS levels at peak systole for healthy, calcified and severely calcified models. Top three snapshots are absolute pressure contours at peak systole. Calcification results in a significant increase in transvalvular pressure gradient TPG (%188 increase for calcified and (%305 increase for severely calcified cases). Bottom three snapshots are octahedron representation of WSS levels on the leaflets. Calcification increases WSS on the leaflets significantly and tips of the leaflets are exposed to highest WSS for all cases.

amount of calcification increases, WSS levels on the front ventricularis surface increase whereas WSS levels on the back fibrosa surface decrease. Therefore, calcification results in an increase in WSS gradient between two surfaces of the leaflets. We also calculated time averaged and maximum WSS levels on the surfaces for the models. Our findings are summarized in Table 2.

Table 1
Orifice velocity, opening ratio, TPG and WSS levels for the simulations.

	Spatially averaged WSS							
	Young Modulus (MPa)	Maximum Jet Velocity (m/s)	Maximum Orifice Diameter (mm)	Maximum Opening ratio (%)	Maximum TPG (Pa)	Cardiac-Averaged (Pa)	Peak Flow (Pa)	Maximum Value (Pa)
Normal	2	1.57	9.0	70.0	633	8.7	13.3	46.7
Calcified	10	2.18	10.5	52.5	1995	10.3	17.5	62.8
Severely calcified	20	2.38	14.0	45.0	2559	12.5	22.5	140.1

Table 2
Spatially Averaged WSS levels on front ventricularis and back fibrosa surfaces for the simulations.

	Cardiac-averaged (Pa)		Peak flow (Pa)		Maximum value (Pa)	
	Front Ventricularis	Back Fibrosa	Front Ventricularis	Back Fibrosa	Front Ventricularis	Back Fibrosa
Normal	16.2	3.1	27.5	18.3	65.6	13.2
Calcified	22.2	1.1	39.7	5.1	80.4	28.1
Severely calcified	25.8	1.3	46.5	4.5	95.1	32.3

4. Discussion

CFD modeling has emerged as a useful approach to investigate aortic valve hemodynamics in diseased cases. Potentially, patient specific CFD models can be used to calculate hemodynamic stress levels as well as flow patterns more accurately than current approaches. This information is critical to assess severity of the defect and can be used to investigate the mechano-biological mechanisms that play role in the progression of the disease. Computational modeling of the aortic valve is very difficult because of the transient behavior of the problem, moving structural zones (leaflets) and counter-interactions between flowing blood and deforming leaflets. For accurate results, FSI approach needs to be adapted. Traditionally, FSI models are generated using custom codes and algorithms. These are difficult to be adopted by other researchers. More recently, commercial softwares provide modules to enable FSI. In the present work, we used ANSYS for simulating hemodynamics through aortic valve. We are providing our strategy in details in the Methods section, which will enable it to be adopted by other interested researchers (Figs. 1 and 2).

As an example case, we investigated the influence of leaflet calcification on aortic valve hemodynamics. For the healthy valve model, velocity contour snapshots at different time-points in the cardiac cycle show high WSS on the ventricularis at peak systole (Fig. 4). For the same model, velocity streamline snapshots (Fig. 5) demonstrate circulatory flow regions within sinuses in late cycle (while the valve is closing). We could determine the direction of the circulatory flows within sinuses from velocity vector representation (Fig. 6). The direction of the vortices is counterclockwise in the upper sinus and clockwise in the lower sinus. These directions do not change throughout the cardiac cycle. Therefore, WSS acting on the fibrosa surface is uni-directional but not bi-directional as suggested by most previous studies [46]. These results are in agreement with a recent experimental work on aortic valve hemodynamics where authors also visualized WSS on the fibrosa of aortic valve as unidirectional [2]. Our preliminary findings from our 3D valve models also show a unidirectional flow within sinuses, suggesting native aortic valve flows having such flow characteristics.

Next, we modeled a calcified valve (10 MPa leaflet Young Modulus) and a severely calcified valve (20 MPa Young Modulus) to compare opening ratio, orifice jet velocity, flow profiles, WSS and TPG levels with healthy valve model (2 MPa Young Modulus). Opening ratios decreased from 70% for the healthy valve to 52.5% for the calcified valve and 45% for the severely-calcified valve, showing calcification results in stenosis (Fig. 7, top). These reductions in valve orifice diameters for calcified valves are expected to increase TPG values for these valves. There were bigger but distorted vortices in calcified valves compared to normal one at peak systole (Fig. 7, middle and bottom). The vortices for the calcified models were further away from the leaflets. While the vortices for the normal valve persist while the valve was closing, the vortices for the calcified valves deteriorate (See Supplemental Movies 1,2 and 3 for the streamline animations for the three models for a complete cardiac cycle). Vortex formations in the sinuses were shown to be important in efficient closure of leaflets [13]. Therefore, vortex deterioration suggests disturbance in leaflet closure in calcification, which might result in regurgitation for calcified valves during negative pressure gradient at diastole.

Compared to healthy valve, calcification increased TPG significantly: %188 for the calcified, and %305 for the severely calcified models (Fig. 8, top). Average WSS on the leaflets also increased significantly; % 32 for the calcified, and %69 for the severely calcified models. Highest WSS is localized to leaflet tips in all cases. Previous studies suggested that, the differences in WSS levels in front and backsides of the leaflets also influence formation of calcification [44,45]. To reveal stress variations in our models, we calculated WSS levels on ventricularis and fibrosa sides separately. These results show that, as the amount of calcification increase, WSS levels on the front ventricularis surface increase whereas WSS levels on the back fibrosa surface decrease. Therefore, when valve leaflet start to calcify, because of the flow disturbance, WSS gradient between two surfaces of the leaflet increases, which might trigger mechano-biological mechanisms for further calcification. As far as we know, this is the first time such a finding is presented. Future work should focus on the influence of WSS gradients for the leaflets on the biology of the cells within the leaflets and association of such cellular responses with valve diseases.

There were few limitations in the study. The computational model that presented here is a 2D model and hence does not represent the native case fully. Our aim in this study was to provide a methodology for aortic valve modeling using a commercial package. This methodology can be applied for 3D modeling in future studies. The limitation in 3D FSI modeling is the requirement of extensive computational power. We are currently working on 3D aortic valve models with optimized mesh densities and reasonable simulation times using ANSYS. Another limitation in the study is using linear elastic material properties for the leaflets and employing uniform calcification for the leaflets for the calcified models. We are currently working on 3D non-homogeneous and anisotropic valve models. Our future models will incorporate dynamics of aortic root to make full FSI aortic valve models. Aortic root diameters were shown to change as much as 10% during ventricular systole to facilitate efficient ejection of blood [47]. This behavior is discussed previously by our group as the active dynamism in valve function [48]. Adaptation of root behavior as prescribed movements will lead to more accurate hemodynamics and leaflet movement simulations. Our validation approach is based on a qualitative leaflet movement comparison of echo images and simulations. This is due to the scarcity of available in-vivo data. In our models, we did not include coronary flows. Finally, in the future, we will study the influence of various physiological flows on valve cusp stiffness by developing patient-specific models. Previously we showed that shear stress responsive pathways (endothelial derived nitric-oxide and endothelin-1) regulate the stiffness of aortic cusps under physiological flow conditions [49]. This finding suggest there is a reciprocal interaction between hemodynamic forces and leaflet stiffness. The precise physiological significance of alterations of the aortic valve stiffness on hemodynamics and associated biological signals need to be explored.

In conclusion, this study presents an easily adaptable FSI modeling methodology to investigate disturbed hemodynamics for aortic valve diseases.

Conflict of interest

None.

Acknowledgements

This research was supported by a Marie Curie International Reintegration Grant within the Seventh European Community Framework Programme (IRG276987 to HCY) and by The Scientific and

Technological Research Council of Turkey, Tubitak (112M148 to HCY and 112M895 to HCY).

References

[1] Maleki H. Structural and fluid-structure interaction analysis of stenotic aortic valves: application to percutaneous aortic valve replacement. Concordia University; 2010.

[2] Yap CH, Saikrishnan N, Tamilselvan G, Yoganathan AP. Experimental measurement of dynamic fluid shear stress on the aortic surface of the aortic valve leaflet. Biomech. Model Mechanobiol 2012;11(1–2):171–82.

[3] Butcher JT, Penrod AM, García AJ, Nerem RM. Unique morphology and focal adhesion development of valvular endothelial cells in static and fluid flow environments. Arterioscler Thromb Vasc Biol 2004;24(8):1429–34.

[4] Butcher JT, Simmons CA, Warnock JN. Mechanobiology of the aortic heart valve. J Heart Valve Dis 2008;17(1):62–73.

[5] Siu SC, Silversides CK. Bicuspid aortic valve disease. J Am Coll Cardiol 2010; 55(25):2789–800.

[6] Stewart BF, Siscovick D, Lind BK, Gardin JM, Gottdiener JS, Smith VE, Kitzman DW, Otto CM. Clinical factors associated with calcific aortic valve disease. Cardiovascular Health Study. J Am Coll Cardiol 1997;29(3):630–4.

[7] Otto CM, Prendergast B. Aortic-valve stenosis — from patients at risk to severe valve obstruction. N Engl J Med 2014;371(8):744–56.

[8] Stewart SF, Nast EP, Arabia FA, Talbot TL, Proschan M, Clark RE. Errors in pressure gradient measurement by continuous wave Doppler ultrasound: type, size and age effects in bioprosthetic aortic valves. J Am Coll Cardiol 1991;18(3):769–79.

[9] Garcia D, Pibarot P, Landry C, Allard A, Chayer B, Dumesnil JG, Durand LG. Estimation of aortic valve effective orifice area by Doppler echocardiography: effects of valve inflow shape and flow rate. J Am Soc Echocardiogr 2004;17(7): 756–65.

[10] Shadden SC, Astorino M, Gerbeau JF. Computational analysis of an aortic valve jet with Lagrangian coherent structures. Chaos 2010;20(1), 017512.

[11] Winslow RL, Trayanova N, Geman D, Miller MI. Computational medicine: translating models to clinical care. Sci Transl Med 2012;4(158):158rv11. 158rv11.

[12] Youssefi P, Gomez A, He T, Anderson L, Bunce N, Sharma R, Figueroa CA, Jahangiri M. Patient-specific computational fluid dynamics—assessment of aortic hemodynamics in a spectrum of aortic valve pathologies. J Thorac Cardiovasc Surg. 153(1): pp. 8–20.e3.

[13] Balachandran K, Sucosky P, Yoganathan AP. Hemodynamics and mechanobiology of aortic valve inflammation and calcification. Int J Inflam 2011, 263870. 2011.

[14] Fedele M, Faggiano E. A patient-specific aortic valve model based on moving resistive immersed implicit surfaces. 2017.

[15] Youssefi P, Gomez A, He T, Anderson L, Bunce N, Sharma R, Figueroa CA, Jahangiri M. Patient-specific computational fluid dynamics-assessment of aortic hemodynamics in a spectrum of aortic valve pathologies. J Thorac Cardiovasc Surg 2017;153(1):8–20. e3.

[16] Bahraseman HG, Languri EM, Yahyapourjalaly N, Espino DM. Fluid-structure interaction modeling of aortic valve stenosis at different heart rates. Acta Bioeng Biomech 2016;18(3):11–20.

[17] Grande KJ, Cochran RP, Reinhall PG, Kunzelman KS. Stress variations in the human aortic root and valve: the role of anatomic asymmetry. Ann Biomed Eng 1998; 26(4):534–45.

[18] Weinberg EJ, Schoen FJ, Mofrad MRK. A computational model of aging and calcification in the aortic heart valve. PLos One 2009;4(6), e5960.

[19] Halevi R, Hamdan A, Marom G, Mega M, Raanani E, Haj-Ali R. Progressive aortic valve calcification: three-dimensional visualization and biomechanical analysis. J Biomech 2015;48(3):489–97.

[20] De Hart J, Peters GW, Schreurs PJ, Baaijens FP. A two-dimensional fluid-structure interaction model of the aortic valve [correction of value]. J Biomech 2000;33(9): 1079–88.

[21] Chandra S, Rajamannan NM, Sucosky P. Computational assessment of bicuspid aortic valve wall-shear stress: implications for calcific aortic valve disease. Biomech Model Mechanobiol 2012;11(7):1085–96.

[22] Halevi R, Hamdan A, Marom G, Lavon K, Ben-Zekry S, Raanani E, Bluestein D, Haj-Ali R. Fluid-structure interaction modeling of calcific aortic valve disease using patient-specific three-dimensional calcification scans. Med Biol Eng Comput 2016; 54(11):1683–94.

[23] Min Yun B, Aidun CK, Yoganathan AP. Blood damage through a bileaflet mechanical heart valve: a quantitative computational study using a multiscale suspension flow solver. J Biomech Eng 2014;136(10):101009.

[24] Vahidkhah K, Azadani AN. Supra-annular Valve-in-Valve implantation reduces blood stasis on the transcatheter aortic valve leaflets. J Biomech 2017;58:114–22.

[25] LaDisa Jr JF, Alberto Figueroa C, Vignon-Clementel IE, Kim HJ, Xiao N, Ellwein LM, Chan FP, Feinstein JA, Taylor CA. Computational simulations for aortic coarctation: representative results from a sampling of patients. J Biomech Eng 2011;133(9), 091008.

[26] Barth T, Jespersen D. The design and application of upwind schemes on unstructured meshes. In: 27th aerospace sciences meeting. American Institute of Aeronautics and Astronautics; 1989.

[27] Jansen K, Shakib F, Hughes TJR. Fast projection algorithm for unstructured meshes. In: Computational nonlinear mechanics in aerospace engineering. American Institute of Aeronautics and Astronautics; 1992. p. 175–204.

[28] Meslem Amina, Bode Florin, Croitoru Cristiana, Nastase Ilinca. Comparison of turbulence models in simulating jet flow from a cross-shaped orifice. Eur J Mech B Fluids 2014;44:100–20.

[29] Tan FP, Soloperto G, Bashford S, Wood NB, Thom S, Hughes A, Xu XY. Analysis of flow disturbance in a stenosed carotid artery bifurcation using two-equation transitional and turbulence models. J Biomech Eng 2008;130(6):061008.

[30] Maleki H, Shahriari S, Durand LG, Labrosse MR, Kadem L. A metric for the stiffness of calcified aortic valves using a combined computational and experimental approach. Med Biol Eng Comput 2014;52(1):1–8.

[31] Ranga A, Mongrain R, Biadilah Y, Cartieer R. A compliant dynamic FEA model of the aortic valve. In: 12th IFToMM world congress; 2007.

[32] Gnyaneshwar R, Kumar RK, Balakrishnan KR. Dynamic analysis of the aortic valve using a finite element model. Ann Thorac Surg 2002;73(4):1122–9.

[33] Benra Friedrich-Karl, Dohmen Hans Josef, Pei Ji, Schuster Sebastian, Wan Bo. A comparison of one-way and two-way coupling methods for numerical analysis of fluid-structure interactions. J Appl Math 2011;2011:16.

[34] Fernández MA, Gerbeau J-F. Algorithms for fluid-structure interaction problems. In: Formaggia L, Quarteroni A, Veneziani A, editors. Cardiovascular Mathematics: modeling and simulation of the circulatory system. Milano: Springer Milan; 2009. p. 307–46.

[35] ANSYS I. ANSYS® academic research, Release 16.2, help System, dynamic mesh update methods. ANSYS, Inc.; 2015.

[36] Galpin PF, Broberg RB, Hutchinson BR. Three- dimensional navier stokes predictions of steady-state rotor/stator interaction with pitch change. In: 3rd annual conference of the CFD, society of Canada, Banff, Alberta. Canada: Advanced Scientific Computing Ltd; 1995.

[37] Weston MW, LaBorde DV, Yoganathan AP. Estimation of the shear stress on the surface of an aortic valve leaflet. Ann Biomed Eng 1999;27(4):572–9.

[38] Garcia D, Pibarot P, Durand LG. Analytical modeling of the instantaneous pressure gradient across the aortic valve. J Biomech 2005;38(6):1303–11.

[39] Keller Eric J, Malaisrie SC, Kruse Jane, van Ooij Pim, Semaan Edouard, McCarthy Patrick, et al. Restoration of physiologic hemodynamics in the ascending aorta following aortic valve replacement: a 4D flow MR study. J Cardiovasc Magn. Reson 2016;18(1):P346.

[40] Dumont K, Stijnen JM, Vierendeels J, van de Vosse FN, Verdonck PR. Validation of a fluid-structure interaction model of a heart valve using the dynamic mesh method in fluent. Comput Methods Biomech Biomed Engine 2004;7(3):139–46.

[41] Moore BL, Dasi LP. Coronary flow impacts aortic leaflet mechanics and aortic sinus hemodynamics. Ann Biomed Eng 2015;43(9):2231–41.

[42] Nishimura Rick A, Otto Catherine M, Bonow Robert O, Carabello Blase A, Erwin John P, Guyton Robert A, et al. AHA/ACC guideline for the management of patients with valvular heart disease: a report of the American college of cardiology/ American heart association task force on practice guidelines. J Am Coll Cardiol 2014;63(22):e57–185. 2014.

[43] Sun L, Rajamannan NM, Sucosky P. Design and validation of a novel bioreactor to subject aortic valve leaflets to side-specific shear stress. Ann Biomed Eng 2011; 39(8):2174–85.

[44] Halevi R, Hamdan A, Marom G, Lavon K, Ben-Zekry S, Raanani E, et al. Fluid-structure interaction modeling of calcific aortic valve disease using patient-specific three-dimensional calcification scans. Med Biol Eng Comput 2016, **54**, (11), 1683–1694.

[45] Mahler GJ, et al. Effects of shear stress pattern and magnitude on mesenchymal transformation and invasion of aortic valve endothelial cells. Biotechnol Bioeng 2014;111(11):2326–37.

[46] Sucosky P, Balachandran K, Elhammali A, Jo H, Yoganathan AP. Altered shear stress stimulates upregulation of endothelial VCAM-1 and ICAM-1 in a BMP-4- and TGF-beta1-dependent pathway. Arterioscler Thromb Vasc Biol 2009;29(2):254–60.

[47] RG1 Leyh, Schmidtke C, Sievers HH, Yacoub MH. Opening and closing characteristics of the aortic valve after different types of valve-preserving surgery. Circulation 1999;100(21):2153–60.

[48] Chester AH, El-Hamamsy I, Butcher JT, Latif N, Bertazzo S, Yacoub MH. The living aortic valve: from molecules to function. Glob Cardiol Sci Pract 2014;2014(1): 52–77.

[49] El-Hamamsy I, Balachandran K, Yacoub MH, Stevens LM, Sarathchandra P, Taylor PM, et al. Endothelium-dependent regulation of the mechanical properties of aortic valve cusps. J Am Coll Cardiol 2009;53(16):1448–55.